COMPUTATIONAL FLUID DYNAMICS SIMULATION OF THE COMBUSTION PROCESS, EMISSION FORMATION AND THE FLOW FIELD IN AN IN-DIRECT INJECTION DIESEL ENGINE

by

Ramin BARZEGAR [a*], ***Sina SHAFEE*** [b], ***and Shahram KHALILARYA*** [c]

[a] Young Researchers Club, Parsabad Mogan Branch, Islamic Azad University, Parsabad, Iran
[b] Department of Mechanical Engineering, Faculty of Natural and Applied Sciences, Middle East Technical University, Ankara, Turkey
[c] Mechanical Engineering Department, Urmia University, Urmia, Iran

Original scientific paper
DOI: 10.2298/TSCI111218108B

In the present paper, the combustion process and emission formation in the Lister 8.1 in-direct injection diesel engine have been investigated using a computational fluid dynamics code. The utilized model includes detailed spray atomization, mixture formation and distribution model which enable modeling the combustion process in spray/wall and spray/swirl interactions along with flow configurations. The analysis considers both part load and full load states. The global properties are presented separately resolved for the swirl chamber (pre-chamber) and the main chamber. The results of model verify the fact that the equal amount of the fuel is burned in the main and pre-chamber at full load state while at part load the majority of the fuel is burned in the main chamber. Also, it is shown that the adherence of fuel spray on the pre-chamber walls is due to formation of a stagnation zone which prevents quick spray evaporation and plays an important role in the increase of soot mass fractions at this zone at full load conditions. The simulation results, such as the mean in-cylinder pressure, heat release rate and exhaust emissions are compared with the experimental data and show good agreement. This work also demonstrates the usefulness of multi-dimensional modeling for complex chamber geometries, such as in in-direct injection diesel engines, to gain more insight into the flow field, combustion process, and emission formation.

Key words: *in-direct injection diesel engine, computational fluid dynamics, flow field, combustion, NO_x, soot*

Introduction

In a very competitive world, improvement of engine performance has become an important issue for automotive manufacturers. In order to improve the engine performance, detailed studies are carried out on combustion process and emission formation. There are two common methods in the field of engine research; experimental study and mathematical simulations (thermo dynamical modeling, computational fluid dynamics (CFD) modeling, *etc*.).

The experimental methods obtain principal and valuable information, but they require costly equipment and are mostly time consuming. The other approach which has become a dominant factor in the engine research in the recent years is the application multi-dimensional CFD codes which can gain insight into the in-cylinder flow field and combustion process by solving the governing flow field and species transport equations [1, 2].

* Corresponding author; e-mail: barzegar@iaupmogan.ac.ir

Diesel engines are preferable to gasoline engines because of their high thermodynamic performance and low HC, CO, and NO_x emissions. The main problem in diesel combustion though is the soot formation, or smoke, which is produced when there is insufficient air for complete combustion [3-6]. In an in-direct injection (IDI) diesel engine, the combustion chamber is divided into two major parts: the pre-chamber and the main chamber which are linked by a throat. In an IDI diesel engine, fuel injects into the pre-combustion chamber and air is pushed through the narrow passage on the compression stroke and becomes turbulent within the pre-chamber. This narrow passage speeds up the expanding gases more. The pre-chamber approximately includes 50% of the combustion volume when the piston is at top dead centre (TDC). This geometry adds an additional difficulty to those to deal with in the direct injection (DI) combustion chambers. Generally speaking, IDI engines have lower performance than DI engines, which is because of their intense heat loss in swirl chamber throat [7]. 3-D modeling takes into account the interactions between different phenomena including turbulent flow, spray, combustion and naturally the geometry of combustion chamber. It allows a precise investigation of the problem as it provides all required properties at any one point within the combustion chamber at any one time. When applied to IDI engines, these models have to address specific problems linked to the flow unsteadiness, high Reynolds numbers involved, and the complex variable geometry of the solid boundaries.

As a consequence, the CFD simulations usually take long calculation time requiring high memory capacity, but these problems have been partially solved as a result of the significant improvement in power and speed of modern computers in recent years. In other words, simulation of the combustion system by means of computer modeling makes it possible to explore combustion regimes that may be difficult and/or expensive to achieve with experiments [8].

There are many reports on experimental studies regarding the IDI diesel engines in the literature such as study of alternative fuels, improving of combustion process and emission reduction [9-13]. Hotta *et al*. [14] worked on an experimental research to reduce the particulate matter (PM) from IDI diesel engine and examined the reducing mechanisms using an optically accessible engine at Toyota central research and development laboratories, Inc. It is now commonly admitted that the design of IDI combustion chambers has to rely more on fundamental knowledge of local aspects which require multi-dimensional simulation. Many fundamental aspects concerning CFD simulation of IDI engines have been discussed earlier by Pinchon [15]. 3-D modeling of combustion process and soot formation in an IDI diesel engine have also been studied by Zellat *et al*. [16] using KIVA code. Strauss and Schweimer [17], at Volkswagen AG, had studied the combustion and pollutant formation processes in a 1.9 l IDI diesel engine using SPEED CFD code for the part load and full load conditions.

Study of the relevant literature shows that only few attempts have been done in order to use the multi-dimensional modeling in IDI diesel engine research up to now. At present work, the AVL Fire CFD code has been used to predict and investigate the flow field, combustion process, performance parameters and emissions in the Lister 8.1 IDI diesel engine at full and part loads. Taking into account the rather complicated nature of the IDI diesel engines due to the continuous mass and energy exchange between the two chambers, we have decided to make an investigation on in-direct injection diesel engine.

Initial and boundary conditions

Calculations are carried out on a closed system from intake valve closure (IVC) at 165° CA bTDC to exhaust valve opening (EVO) at 180° CA aTDC. Figure 1 shows the numerical grid, which is designed to model the geometry of the engine and contains a maximum of

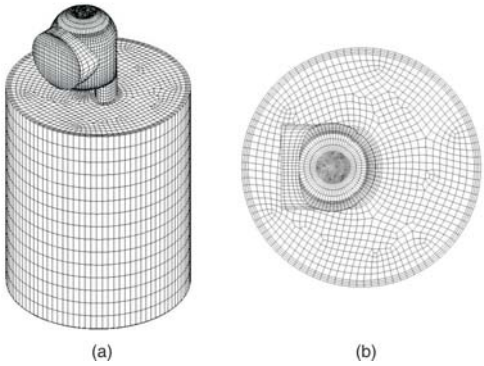

Figure 1. (a) Mesh for the Lister 8.1 IDI diesel engine; (b) top view of the mesh

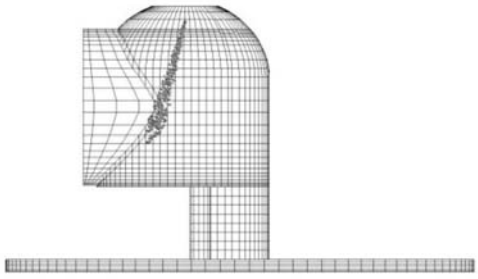

Figure 2. Spray and injector co-ordination at pre-chamber

42200 cells at 165° CA bTDC. The present resolution was found to give adequately grid independent results. The diesel fuel is injected via a single hole injector in pre-chamber as shown in fig. 2. Initial conditions for pressure and temperature in the combustion chamber are 86 kPa and 384 K, respectively, and swirl ratio is assumed to be at quiescent condition. The engine speed under study is 730 rpm. for both full load and part load states. All boundary temperatures were assumed to be constant throughout the simulation, but allowed to vary at combustion chamber surfaces.

Model description

The specifications of the Lister 8.1 IDI diesel engine are listed on tab. 1. The flow was solved from IVC to EVO using the AVL FIRE CFD code [18]. The AVL CFD code is powerful software which is used by researches in internal combustion engine field and car manufacturers to investigate different aspects of combustion and emission formation in engines. This code solves the compressible, turbulent, 3-D transient conservation equations for reacting multi-component gas mixtures with the flow dynamics of an evaporating liquid spray. The turbulent flow within the combustion chamber is simulated using the RNG k-ε turbulence model, modified for variable-density engine flows [19].

Table 1. Specifications of Lister 8.1 IDI diesel engine

Cycle type	Four stroke
Number of cylinders	1
Injection type	IDI
Cylinder bore	114.1 mm
Stroke	139.7 mm
L/R (rod/stroke ratio)	2
Displacement volume	1.43 litre
Compression ratio	17.5:1
$V_{pre\text{-}chamber}/V_{TDC}$	0.7
Full load injected mass	6.4336e-5 kg per cycle
Part load injected mass	3.2009e-5 kg per cycle
Max power on 850 rpm	8 hp
Max power on 650 rpm	6 hp
Injection pressure	91.7 kg/cm^3
Start injection timing	20° bTDC
Nozzle diameter at hole center	0.003 m
Number of nozzle holes	1
Nozzle outer diameter	0.0003 m
Spray cone angle	10°
Valve timing	IVO = 5° bTDC
	IVC = 15° ABDC
	EVO = 55° BBDC
	EVC = 15° aTDC

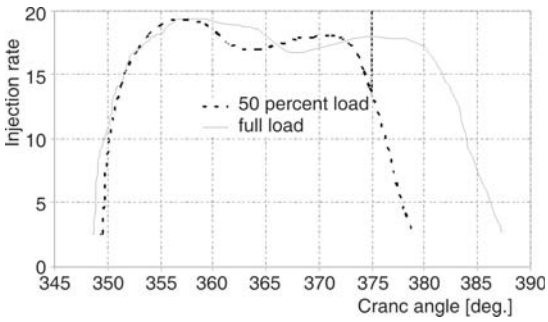

Figure 3. Part load and full load injection histories

The standard WAVE model [20] is used for the primary and secondary atomization modeling of the resulting droplets. At this model the growth of an initial perturbation on a liquid surface is linked to its wave length and other physical and dynamical parameters of the injected fuel at the flow domain. Drop parcels are injected with characteristic size equal to the Nozzle exit diameter (blob injection). The injection rate profiles at full load state and 50% load are shown in fig. 3.

The Dukowicz model is applied for treating the heat up and evaporation of the droplets, which is described in [21]. This model assumes a uniform droplet temperature. In addition, the droplet temperature change rate is determined by the heat balance, which states that the heat convection from the gas to the droplet either heats up the droplet or supplies heat for vaporization. A Stochastic dispersion model was employed to take the effect of interaction between the particles and the turbulent eddies into account by adding a fluctuating velocity to the mean gas velocity [18].

The spray/wall interaction model used in this simulation was based on the spray/wall impingement model [22] which has previously been utilized by authors to investigate effects of fuel injection mode and spray impingement on diesel combustion [1, 2]. The Shell auto- -ignition model was used for modeling of the auto ignition [23]. In this generic mechanism, six generic species for hydrocarbon fuel, oxidizer, total radical pool, branching agent, intermediate species, and products were involved. In addition the important stages of auto ignition such as initiation, propagation, branching and termination were presented by generalized reactions, described in [18, 23]. The Eddy break-up model (EBU) based on the turbulent mixing was used for modeling of the combustion in the combustion chamber [18]. NO_x formation is modeled by the Zeldovich mechanism and soot formation is modeled by Kennedy, Hiroyasu, and Magnussen mechanism [24].

Results and discussion

The calculations are carried out for the single cylinder Lister 8.1 IDI diesel engine and the operating conditions are full and 50% load at constant speed of 730 rpm. Figures 4 and 5 show the comparison of computed and measured [25] mean in-cylinder pressure and heat release rate (HRR,) respectively, for both load cases. The good agreement between measured and predicted data especially during the compression and expansion strokes verifies the model. Both premixed and diffusion combustion phases are computed as well. Comparing these figures also shows the effect of load on the heat release rate and in-cylinder pressure. The measured HRR curve is derived from the first law analysis of procured in-cylinder pressure data as:

$$\frac{\mathrm{d}Q}{\mathrm{d}\theta} = \frac{\gamma}{\gamma - 1} p \frac{\mathrm{d}V}{\mathrm{d}\theta} + \frac{1}{\gamma - 1} V \frac{\mathrm{d}P}{\mathrm{d}\theta} \tag{1}$$

In this equation, P and V are in-cylinder pressure and volume *vs*. crank angle θ, and $\gamma =$ = 1.35. The results presented in the figures are global (cylinder averaged) quantities as a function of time (crank angle). In order to study the part load condition, only the fuel injection timing and amount of injected mass were changed and the rest of the initial conditions were unaffected.

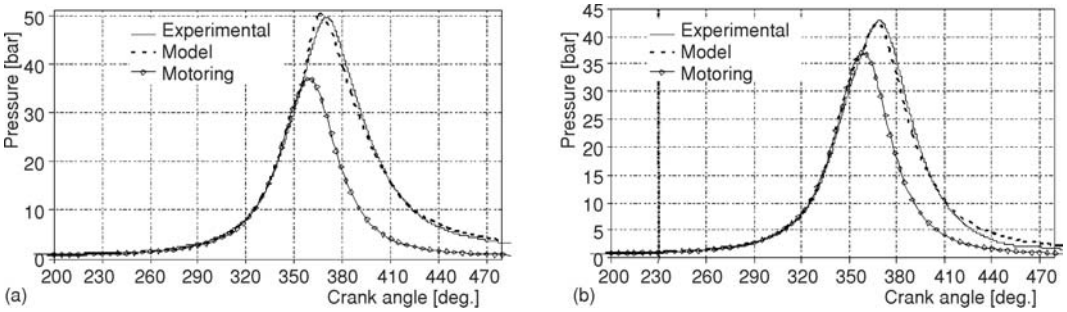

Figure 4. Comparison of measured [23] and calculated pressure at 730 rpm for (a) full load and (b) part load

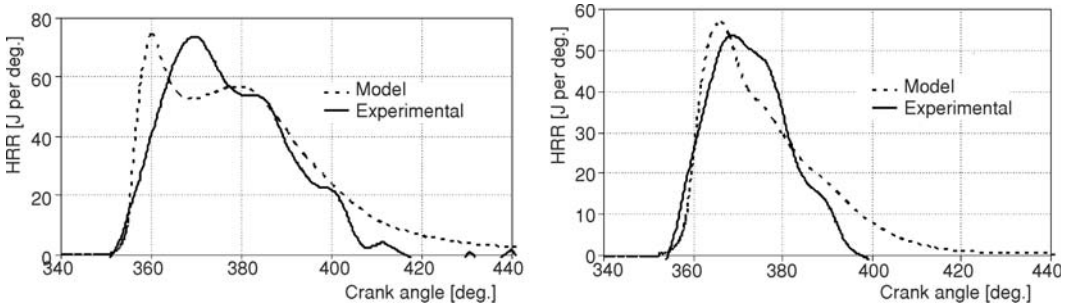

Figure 5. Comparison of experimental and calculated heat release rate at 730 rpm for (a) full load and (b) part load

The peak pressures discrepancy between experiment and computation is less than 0.2%. Increasing load to full load mode causes in-cylinder peak pressure to increase to 50.2 bar from 42.3 bar and ignition delay decreased to 7.9 crank angle degree (CAD) from 10.7 CAD with respect to 50% load. At full load operation, due to injection of fuel in later parts of cycle and also longer injection duration, much of the fuel is burned in diffusion phase. Figure 4 also shows the quantity of computational and experimental results for start of combustion (SOC) and ignition delay (ID) CAD in both cases. The discrepancies of SOC or ID between computation and experiment at part load and full load operation are as small as 0.8° and 0.1° crank angle, respectively. Figure 6 shows the development of the burnt mass fraction. There is a classic result found in re-

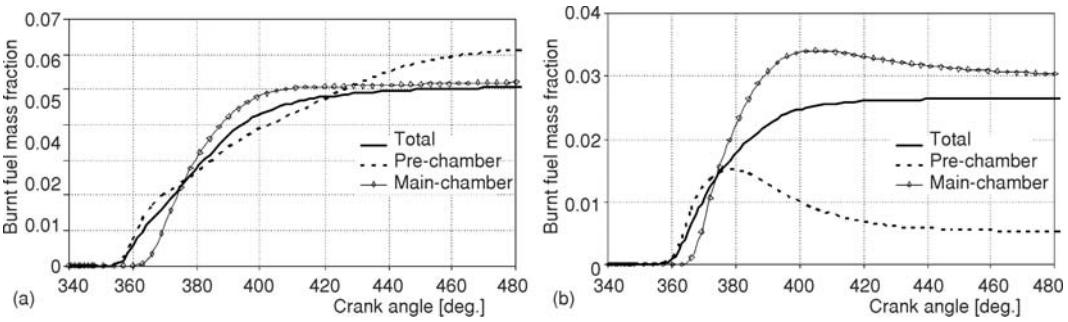

Figure 6. Calculated burn fuel mass fraction at 730 rpm for (a) full load and (b) part load

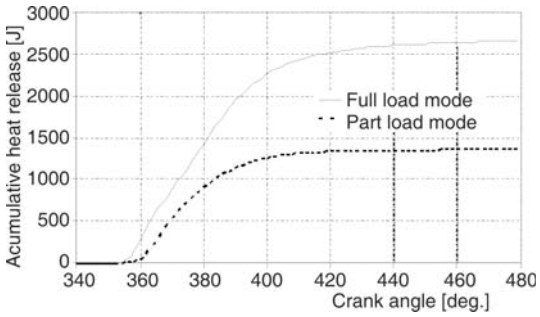

Figure 7. Accumulated heat release rate at 730 rpm for full and part load operations

lation between the values for the main and the pre-chamber burnt fuel mass. It can be seen that the SOC is earlier in the full load state compared with the part load case in the pre-chamber. Also at full load state, the computed burn fuel mass fraction and heat release rate are equality shared between the main chamber and pre-chamber. This shows that simulations have correctly represented a typical feature at part load states in IDI combustion with fuel burning mostly in the main chamber. Figure 7 also indicates the accumulated heat release rate at full and part load operations.

The mean in-cylinder temperature histories are presented region-resolved for the swirl, main and total in-cylinder chamber in fig. 8. The peak temperature values in the swirl chamber, main chamber, and in total occur, respectively, at 1394, 1612, and 1389 K for part load and 1788, 1966, and 1827 K for full load operation, respectively. With the increase of load at constant speed (730 rpm) from, the peak temperature in swirl, main and total in-cylinder chambers increase by 394, 354, and 438 K, respectively. The increase in load means an increase in the equivalence ratio since the amount of injected fuel is increased for constant air mass in the pre-chamber. This tends to increase the air temperatures and thus increases the chances of forming a flammable mixture for pre-flame reactions to take place.

This reduces the ID in the pre-chamber. Also at full load operation, because of the longer injection duration, combustion period is longer than the part load operation, hence, temperatures in the swirl, main and total in-cylinder chambers at full load are higher than the 50% part load operation in the expansion stroke. Also in the IDI diesel engine, since the fuel spray is injected into an auxiliary chamber such as the swirl chamber, most of the fuel spray will remain in the pre-chamber, especially at full load operation. The impinged fuel gradually evaporates and burns. Therefore combustion period in pre-chamber is long at full load operation, fig. 8(a).

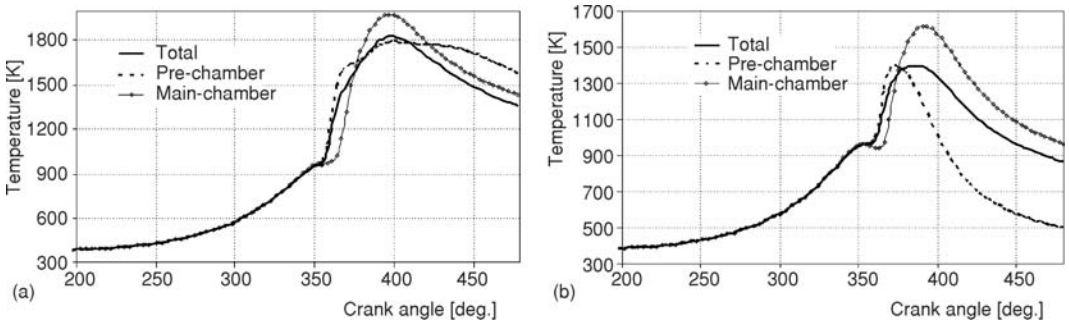

Figure 8. Comparison of experimental and calculated heat release rate at 730 rpm for (a) full load and (b) part load

Figure 9 represents vectors of the velocity field at various crank angles in horizontal cuts from main combustion chamber and planes across the connecting throat. It was found out that the maximum velocities obtained here were lower than the corresponding data in the litera-

ture [7, 14-16] due to large areas at throat section. The maximum velocity for full load operation is then 56 m/s at 10° CA aTDC which is a result of start of combustion occurring in pre-chamber and maximum mass outflow. Figure 8 also indicates that the swirl generated during the compression stroke (20° CA bTDC at fig. 9) becomes gradually weaker due to opposite flow in glow plug. At 60° CA aTDC, velocities get dominated by the evacuation of pre-chamber. The flow in throat changes its direction at the beginning of combustion and after TDC the flow in the pre-chamber is strongly influenced by the fuel spray. The top view corresponding to 20° CA aTDC depicts the formation of two vortices which are created by the deceleration of the axial penetration of the mixture. In the front view at 40° CA aTDC, the gas from the pre-chamber reaches the opposite side of cylinder. This leads to the formation of two large eddies each occupying a half of the main chamber and staying centered with respect to the two half of the bowl. At 60° CA aTDC, these eddies are bigger. Flow field at part load operation is similar to full load, whereas that maximum velocity is 61 m/s.

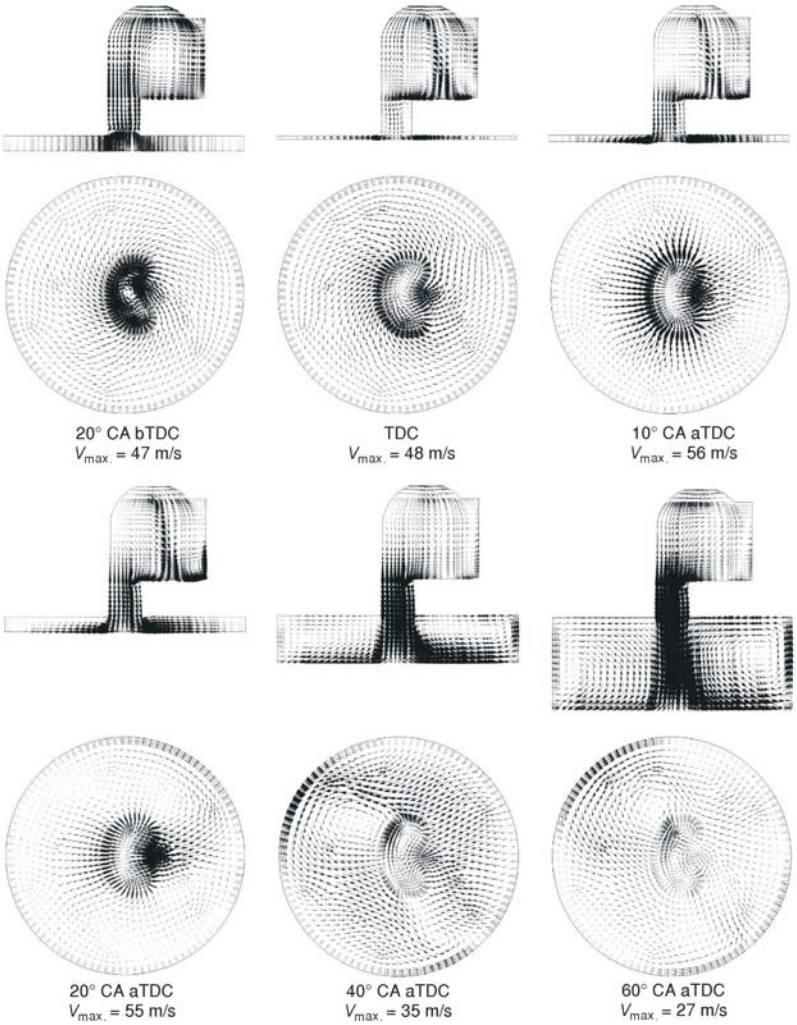

Figure 9. Velocity vector plots for full load operation

In fig. 10, contours of the fuel spray and vapor saturation are presented from start of injection at 10° CA bTDC to 35° CA aTDC. The velocity flow field shown in fig. 9 explains why the spray conserves initial direction imposed by the injector. The fuel vapor-air mixing in the pre-chamber is better in the full load case than the part load condition due to the existence of vortexes at the full load operation. Also, impingement of fuel spray against the chamber wall is a result of less interaction between flow field and spray. It is observed that increased engine load yields in more fuel vaporization and spray droplets in the pre-chamber at the beginning of combustion. This is probably the origin of the much higher soot formation in the pre-chamber at full load operation. The hard spray impingement causes fuel adhesion on the wall near spray-wall impinging point. This adherent fuel is not quickly evaporated and the formed fuel vapor is hardly carried out of this area which is a stagnation zone due to the chamber shape. Thus it is possible that the rich fuel-air mixture stagnates in this zone under the condition of high temperature and insufficient oxygen to form the dense soot cloud.

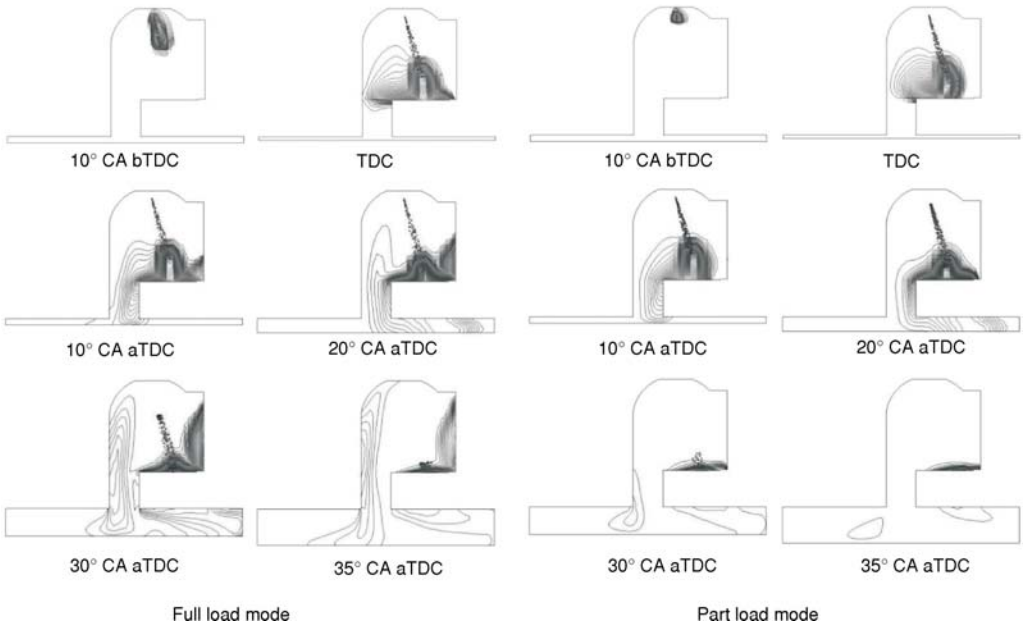

Figure 10. Spray and vapor saturation contours

Performance parameters

Table 2 shows the variation of performance parameters *vs.* load operation, compared with the experimental data [25]. By comparison with the experimental results, it can be seen that the model predictions have a good accuracy. Indicated work per cycle was calculated from the cylinder pressure and piston displacement as:

$$W = \int_{\theta_1}^{\theta_2} P\mathrm{d}V \tag{2}$$

where θ_1, and θ_2 are the start and end of the valve-closed period, respectively, (*i. e.* IVC = 15° aBDC and EVO = 55° bBDC). The indicated power per cylinder and indicated mean effective pressure were related to the indicated work per cycle by:

$$P = \frac{WN}{60000n} \tag{3}$$

$$IMEP = \frac{W}{V_{\mathrm{d}}} \tag{4}$$

where $n = 2$ is the number of crank revolutions for each power stroke per cylinder, N – the engine speed, and V_{d} – the volume displacement. The brake specific fuel consumption (BSFC) was defined as:

$$BSFC = \frac{m_{\mathrm{f}}}{P_{\mathrm{b}}} \tag{5}$$

In eq. 2, the work was only integrated as part of the compression and expansion strokes and the pumping work was not taken into account. Therefore, the power and ISFC analyses can only be viewed as being qualitative rather than quantitative in this study.

Table 2. Performance parameters predictions and compared with experiments

	Part load mode	Full load mode		
	CFD model	Experimental	CFD model	Experimental
Indicated power [kW]	3.006	–	5.773	–
Brake power [kW]	2.555	2.535	4.907	5.064
$\dot{m}_{\mathrm{fuel}}$ [gs^{-1}]	0.196	0.196	0.391	0.391
BMEP [bar]	2.98	2.96	5.72	5.90
BSFC [gkW^{-1}h^{-1}]	276	277	287	278

Emission formation results analysis

In the following section, the production of NO_x and soot as main emissions in IDI diesel engines are discussed. Exhaust NO_x values are compared and verified with experimental data for both cases. Comparison shows that the predicted values are in good agreement with measured data for the full load operation case while at part load operation there is diversity between results. As the fuel injection is retarded, the time available for air/fuel mixing and combustion is reduced, and the consumption rate of the fuel decreases. The fuel consumption rate becomes much slower with very late injection, resulting in significant increases in the unburned fuel amount.

As indicated by fig. 11, under medium and high load conditions, the main cause of the exhaust smoke can be both the fuel adhesion to the chamber wall and stagnation of rich fuel-air mixture. Also it can be seen that the NO_x formation is intensified in areas with equivalence ratio close to 1 and the temperature higher than 2000 K. In addition to this, the area which the equivalence ratio is higher than 3 and the temperature is approximately between 1600 K and 2000 K yields in greater soot concentration. A local soot-NO_x trade-off is evident in these contour plots where the NO_x and soot formation occur on opposite sides of the high temperature region [26]. The in-cylinder temperature histories reveal that the flame started in pre-chamber and then invades a large portion of the main-chamber very quickly. It is observed that the beginning of the

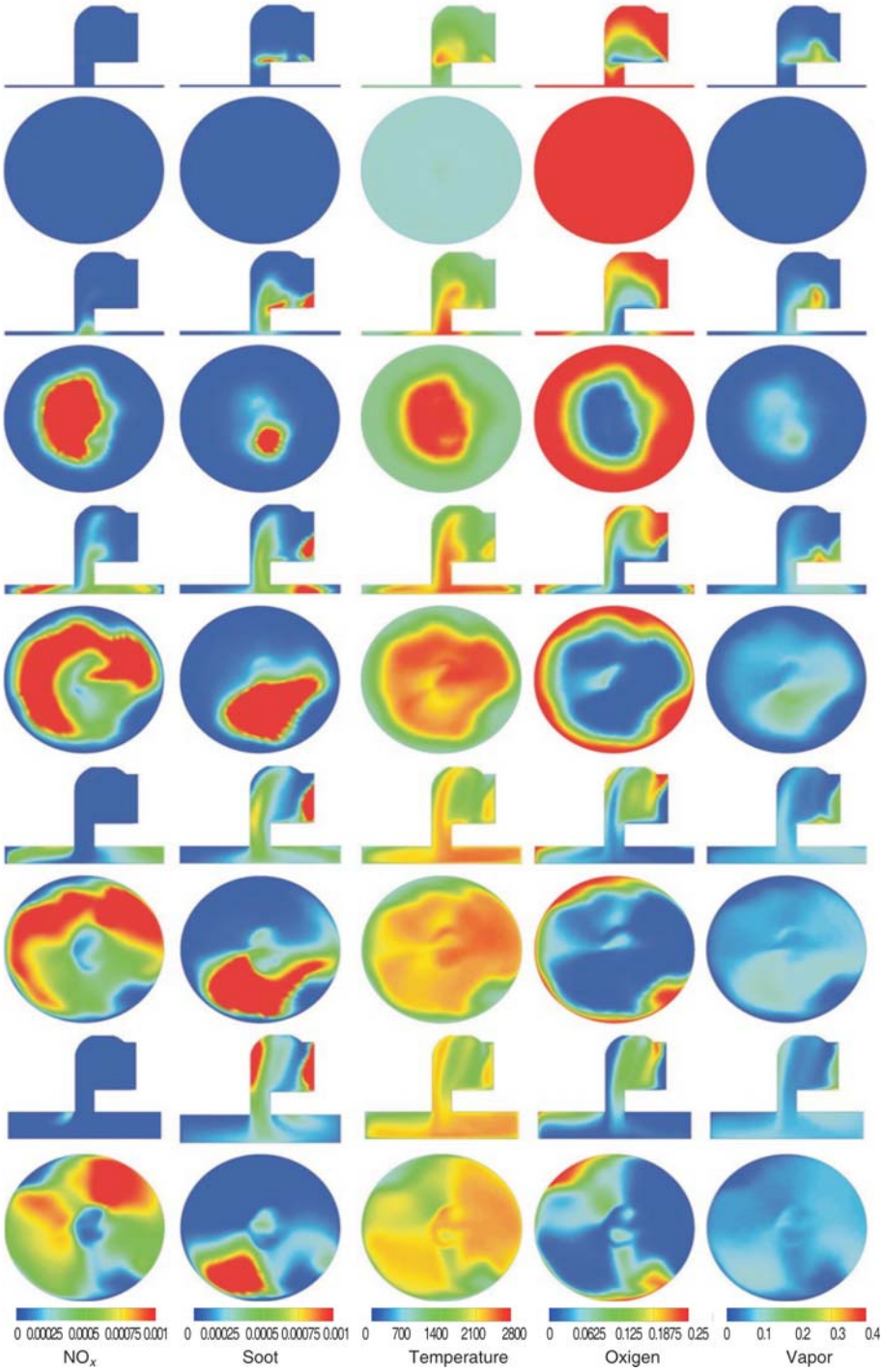

Figure 11. NO_x, soot, temperature, oxygen, and vapor mass fractions contour plots at full load operation (from left to right) for TDC, 10°, 20°, 30°, and 40° CA aTDC (from top to bottom)
(for color image see journal web site)

mass transfer between pre-chamber and the main chamber is around TDC. The development of the temperature field between 20° and 30° CA aTDC shows that the axial and the radial penetrations of the flame front are almost equal. Thus, the flame front reaches the lateral cylinder wall and the cylinder wall opposite to the pre-chamber at approx. the same time. The fast decrease of the oxygen concentration in main and pre-chambers correspond to a large high temperature zone (over 2000 K at 10° CA aTDC).

The region resolved global NO_x formation of for the two cases are given in figs. 12(a) and 12(b). NO_x formation starts off at about 17° CA for full load and 18° CA for part load operation state after the start of injection. The initial increase in the global NO_x formation follows the global temperature trend (also on fig. 8). Also it is observed that NO_x formation in main chamber is higher compared to that in pre-chamber especially at part load operation. Finally, figs. 12(c) and 12(d) present the evolution of the soot in the chamber and in the pre-chamber for both load conditions. One could notice that at part load, the maximum soot mass is observed in the main. However, soot oxidation is fast the exhaust gas is already attained at about 60 CA aTDC. In fact, because of the availability of sufficient oxygen, the turbulent soot oxidation diminishes the soot concentrations to 0.1 g/kWh at about 110° CA aTDC. At high loads, soot quantities in the pre-chamber is much bigger than main chamber due to stagnation region forming in glow plug and also soot is produced in regions of high fuel concentrations, where cold fuel is injected into areas of hot gases. The soot is then oxidized again in the leaner regions of the flame, so that most of the soot is already consumed in zones close to the stoichiometric. Soot quantities in the pre-chamber vanish due to its oxidation and convection to the main chamber.

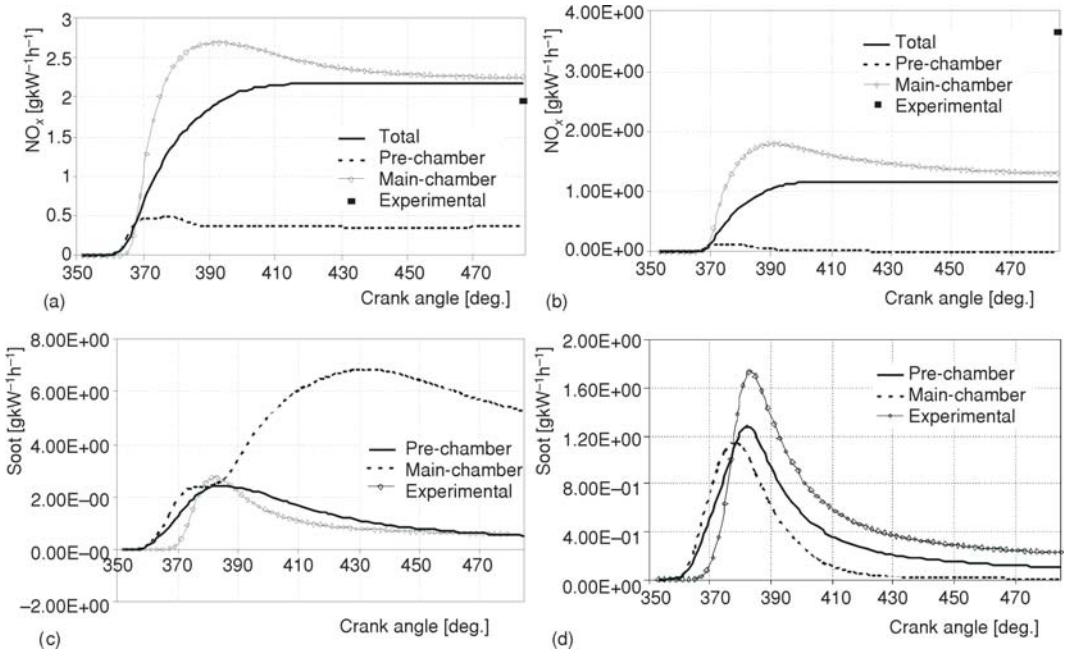

Figure 12. Comparison of measured [23] and calculated exhaust emission at 730 rpm for full load and part load operation

Conclusions

In this paper, the mixture formation, combustion processes, pollutant formation, flow field, and the performance parameters within Lister 8.1 IDI diesel engine were simulated at full load and part load operation conditions. The global properties were presented resolved for the swirl and main chamber separately. As for the interpretation of the results, it was shown that the weak deflection of the fuel jet was because of the low swirl level in the pre-chamber due to the presence of the glow plug. Results for calculated pressure, exhaust emissions and performance parameters were compared with the corresponding experimental data and show good agreement. Such verification between the experimental and computed results gives confidence in the model prediction, and suggests that the model may be used at future works. The CFD simulations have also shown that they greatly improve the understanding and to facilitate the analysis of the combustion and pollutant formation processes in the multi-chamber diesel engines.

Nomenclature

$\dot{m}_f$ – fuel consumption rate, [kgs^{-1}]
N – engine speed, [rpm]
P – mean cylinder pressure, [kPa]
Pb – brake power, [kW]
Pi – indicated pressure, [kPa]
Q – heat released in combustion chamber, [kJ]
V – cylinder volume, [m^3]
V_d – displacement volume[m^3]
W – work per a cycle, [kJ]

Greek symbol

θ – crank angle, [deg.]

Acronyms

aTDC – after top dead centre
BMEP – brake mean effective pressure
BMEP – brake mean effective pressure
BSFC – brake specific fuel consumption
bTDC – before top dead centre
CFD – computational fluid dynamics
DI – direct injection
EBU – eddy brake up
EVO – exhaust valve opening
IDI – in-direct injection
IVC – inlet valve closure
SOC – start of combustion

References

[1] Jafarmadar, S., *et al*., Numerical Investigation of the Effect of Fuel Injection Mode on Spray-Wall Impingement and Combustion Process in a Direct Injection Diesel Engine at Full Load State, *Thermal Science, 14* (2010), 4, pp. 1039-1049, DOI: 10.2298/TSCI10041039J
[2] Jafarmadar, S., *et al*., Modeling the Effect of Spray/Wall Impingement on Combustion Process and Emission in a DI Diesel Engine, *Thermal Science, 13* (2009), 3, pp. 23-33, DOI: 10.2298/TSCI0903023J
[3] Heywood, J. B., Internal Combustion Engine Fundamental, McGraw Hill, New York, USA, 1988
[4] Benson, R. S., Whitehouse, N. D., Internal Combustion Engines, Pergamon Press, Oxford, USA, 1979
[5] Ferguson, C. R., Internal Combustion Engines, John Wiley and Sons, New York, USA, 1986
[6] Obert, E. F., Internal Combustion Engines and Air Pollution, Intext Education Publ., New York, USA, 1993
[7] Patterson, D. J., Henein, N. A., Emissions from Combustion Engines and Their Control, Science Publ., Ann Aebor, Mich., USA, 1972
[8] Uludogan, A., *et al*., Modeling the Effect of Engine Speed on the Combustion Process and Emissions in a DI Diesel Engine, SAE paper 962056, 1996
[9] Sanli, A., *et al*., The Influence of Engine Speed and Load on the Heat Transfer between Gases and In-Cylinder Walls at Fired and Motored Conditions of an IDI Diesel Engine, *Applied Thermal Eng., 28* (2008), 11-12, pp. 1395-1404
[10] Canakci, M., *et al*., Combustion Analysis of Preheated Crude Sunflower Oil in an IDI Diesel Engine, *Biomass and Bioenergy, 33* (2009), 5, pp. 760-767
[11] Selim, M. Y. E., *et al*., Combustion of Jojoba Methyl Ester in An Indirect Injection Diesel Engine, *Renewable Energy*, *28* (2003), 9, pp. 1401-1420

[12] Celikten, I., An Experimental Investigation of the Effect of the Injection Pressure on Engine Performance and Exhaust Emission in Indirect Injection Diesel Engines, *Applied Thermal Eng*., *23* (2003), 16, pp. 2051-2060
[13] Parlak, A., *et al*., The Effects of Injection Timing on NO_x Emissions of a Low Heat Rejection Indirect Diesel Injection Engine, *Applied Thermal Eng*., *25* (2005), 17-18, pp. 3042-3052
[14] Hotta, Y., *et al.*, Combustion Improvement for Reducing Exhaust Emissions in IDI Diesel Engine, SAE paper 980503, 1998
[15] Pinchon, P., Three Dimensional Modeling of Combustion in a Pre-Chamber Diesel Engine, SAE paper 890666, 1989
[16] Zellat, M., *et al*., Three Dimensional Modeling of Combustion and Soot Formation in an Indirect Injection Diesel Engine, SAE paper 900254, 1990
[17] Strauss, T. S., Schweimer, G. W., Combustion in a Swirl Chamber Diesel Engine Simulation by Computation of Fluid Dynamics, SAE paper 950280, 1995
[18] ***, AVL FIRE user manual, Ver. 8.5, 2006
[19] Han, Z., Reitz, R. D., Turbulence Modeling of Internal Combustion Engines Using RNG k-ε Models, *Combust Sci. and Tech., 106* (1995), 4-6, pp. 267-295
[20] Liu, A. B., Reitz, R. D., Modeling the Effects of Drop Drag and Break-up on Fuel Sprays, SAE paper 930072, 1993
[21] Dukowicz, J. K., Quasi-Steady Droplet Change in the Presence of Convection, Informal Report Los Alamos Scientific Laboratory, Los Alamos, N. Mex., USA, LA7997-MS
[22] Naber, J. D., Reitz, R. D., Modeling Engine Spray/Wall Impingement, SAE paper 880107, 1988
[23] Halstead, M., *et al*., The Auto Ignition of Hydrocarbon Fueled at High Temperatures and Pressures – Fitting of a Mathematical Model, *J. Combust Flame, 30* (1977), pp. 45-60
[24] Patterson, M. A., *et al*., Modeling the Effects of Fuel Injection Characteristics on Diesel Engine Soot and NO_x Emissions, SAE paper 940523, 1994
[25] Mohammahi, A., Ignition of Dual Fuel Engines by Using Free Radicals Existing in EGR Gases, Ph. D. thesis, Faculty of Mechanical Engineering, Tabriz University, Tabriz, Iran 2008
[26] Carsten, B., Mixture Formation in Internal Combustion Engines, Springer Publications, Berlin, 2006

Paper submitted: December 18, 2011
Paper revised: April 8, 2012
Paper accepted: April 20, 2012